SANDIA REPORT
SAND2019-2347
Printed March 2019

Sandia National Laboratories

Nishati Prototype 72-Cell Endurance® Modules: Test Report

Bruce H. King, Julius Yellowhair and Charles D. Robinson

Prepared by
Sandia National Laboratories
Albuquerque, New Mexico
87185 and Livermore,
California 94550

Issued by Sandia National Laboratories, operated for the United States Department of Energy by National Technology & Engineering Solutions of Sandia, LLC.

Available to DOE and DOE contractors from
U.S. Department of Energy
Office of Scientific and Technical Information
P.O. Box 62
Oak Ridge, TN 37831

Telephone: (865) 576-8401
Facsimile: (865) 576-5728
E-Mail: reports@osti.gov
Online ordering: http://www.osti.gov/scitech

Available to the public from
U.S. Department of Commerce
National Technical Information Service
5301 Shawnee Rd
Alexandria, VA 22312

Telephone: (800) 553-6847
Facsimile: (703) 605-6900
E-Mail: orders@ntis.gov
Online order: https://classic.ntis.gov/help/order-methods/

ABSTRACT

US Manufacturer Nishati provided three prototype, 72-cell photovoltaic modules to Sandia for characterization under the US Department of Energy Small Business Voucher program. Nishati is developing the Endurance© product to address the stringent requirements associated with PV system installations sited near airports and military bases. These prototype modules are uniquely constructed of a polymeric matrix and an internal honeycomb structural element. Target features of the module design are reduced reflectivity from the front surface and reduced weight.

Sandia applied a variety of in-house characterization methods to these modules with the goal of validating performance and identifying any areas for improvement. Reflectance testing revealed extremely low specular reflection, dramatically surpassing the performance of industry standard PV panels. Electrical performance testing validated performance in line with expectations for similar size and power class modules. Complimentary to reflection testing, outdoor angle of incidence testing indicated performance far exceeding expectations for industry standard PV panels.

It is possible that the extremely low reflectance properties of these modules will convey an advantage in annual energy production in comparison to industry standard modules. Detailed performance modeling and experimental field validation would be required to verify this possible advantage. During the course of this testing, no obvious deficiencies in this module design were discovered. It is recommended that Nishati and Sandia proceed to the final Task associated with the SBV award. This final task will involve fielding modules at Sandia for reliability and energy production validation.

This page left blank

CONTENTS

LIST OF FIGURES

LIST OF TABLES

ACRONYMS AND DEFINITIONS

Abbreviation	Definition
AM	Air Mass
AOI	Angle of Incidence
ARC	Anti-Reflective Coating
DNI	Direct Normal Irradiance
Ee	Effective Irradiance
EL	Electroluminescence
GNI	Global Normal Irradiance
GPOA	Global Irradiance in the Plane of Array
Imp	Current at Maximum Power
Isc	Short Circuit Current
IV	Current-Voltage
NMOT	Normal Module Operating Temperature
NOCT	Normal Operating Cell Temperature
Pmp	Maximum Power
PV	Photovoltaic
RTD	Resistive Temperature Detector
SAPM	Sandia Array Performance Model
SBV	Small Business Voucher
SGHAT	Solar Glare Hazard Assessment Tool
SPP	Strategic Partnerships Project
STC	Standard Test Conditions
Vmp	Voltage at Maximum Power
Voc	Open Circuit Voltage

This page left blank

1. INTRODUCTION

This report documents test results for three modules performed by Sandia National Labs for Nishati under the Department of Energy (DOE) Small Business Voucher (SBV) program and Strategic Partnership Project (SPP) 061160727. This report serves as the deliverable for Task 2 of the project. Each of the modules under test were produced and supplied by Nishati. Testing consisted of glint/glare characterization to determine specular reflectance properties and both indoor and outdoor performance characterization to determine electrical response.

Reflection testing was conducted between 0 and 90° using a red laser and photodetector. The measurement set-up was calibrated to a Surface Optics 410 Solar Reflectometer to scale the results to solar-weighted reflectance. The reflectance data will be incorporated into the GlareGauge tool licensed to ForgeSolar. Indoor performance characterization was performed using an industry standard Spire 4600SLP one sun module flash tester, yielding a Standard Test Conditions (STC) power rating for each module. Outdoor performance characterization was performed under natural sunlight and utilized unique solar tracking capabilities developed by Sandia specifically to support module characterization. All outdoor performance characterization was performed simultaneously, with all modules mounted in the same test plane. Outdoor testing produced coefficients for the Sandia Array Performance Model (SAPM) [1] that can be used for system design and power prediction purposes. Raw measurements are available to Nishati upon request.

2. MODULES

Three modules were provided by Nishati to Sandia in June 2018. Each of these were prototype utility scale (72-cell) modules produced by Nishati. Materials for the prototypes were selected as a result of screening studies performed in Task 1 and consisted of a textured clear coversheet and a white back sheet. Additionally, the modules used a metal honeycomb support structure in place of a traditional metal frame or glass-glass construction. The test devices are listed below in Table 2-1.

Table 2-1. Test Devices

Manufacturer	Model	PVID	Serial Number
Nishati	232286	3405	2260001-00006; M048NS001; SN.003
Nishati	232286	3406	2260001-00009; M048NS001; SN.007
Nishati	232286	3407	2260001-00097; M048NS001; SN.002

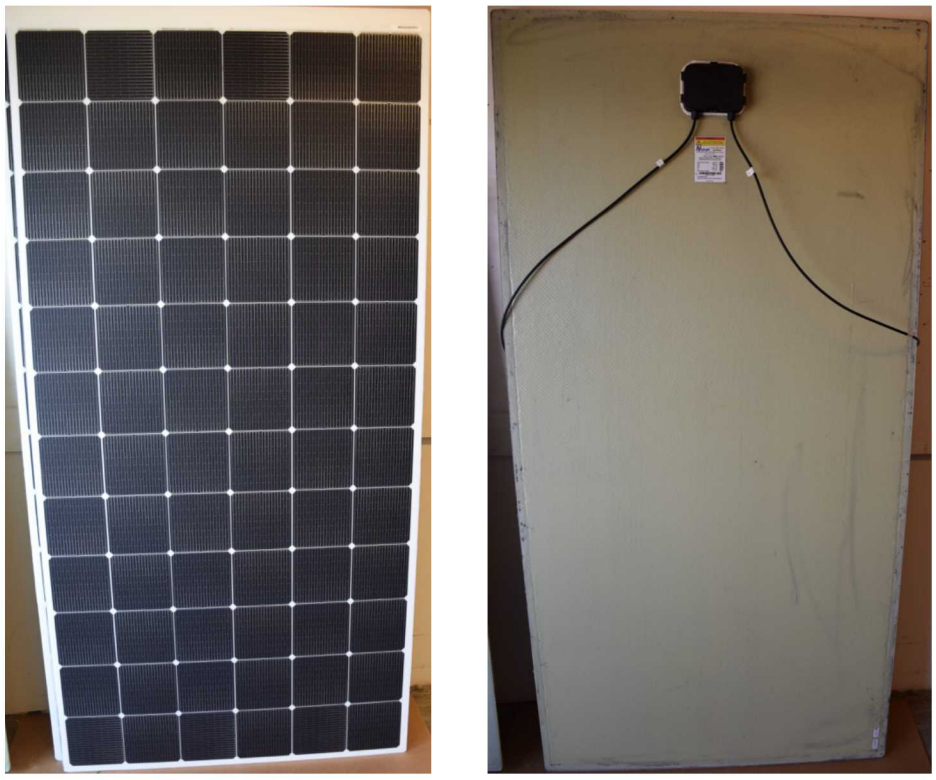

Figure 2-1. Nishati Prototype Endurance Module

3. GLINT/GLARE CHARACTERIZATION

3.1. Measurement Methods

The reflection/angle of incidence measurement set up is shown in Figure 3-1. A solid-state laser (λ = 635 nm) is mounted on a tripod pan-tilt head. The pan-tilt head provides varying angles of incidence of the laser beam. The test sample is placed on a height adjustable table which is leveled. A Leica Disto D8, with a built-in electronic level, is used to level the table as well as set the angle of the laser. A rotating swing arm, which swings from 0° (vertical) to 90° (horizontal), is attached to the table. A photodetector is mounted at the end of the horizontal arm coming off the swing arm. The swing arm angle is set to match the laser incidence angle. The distance of the photodetector from the PV sample surface is set to achieve 6° acceptance angle on the detector. The solid-state red laser is calibrated to a Surface Optics 410-Solar Reflectometer at 20° angle of incidence. The raw laser reflectance data is scaled by the calibration factor to get the solar-weighted specular reflectance at 6° acceptance angle over varying angles of incidence.

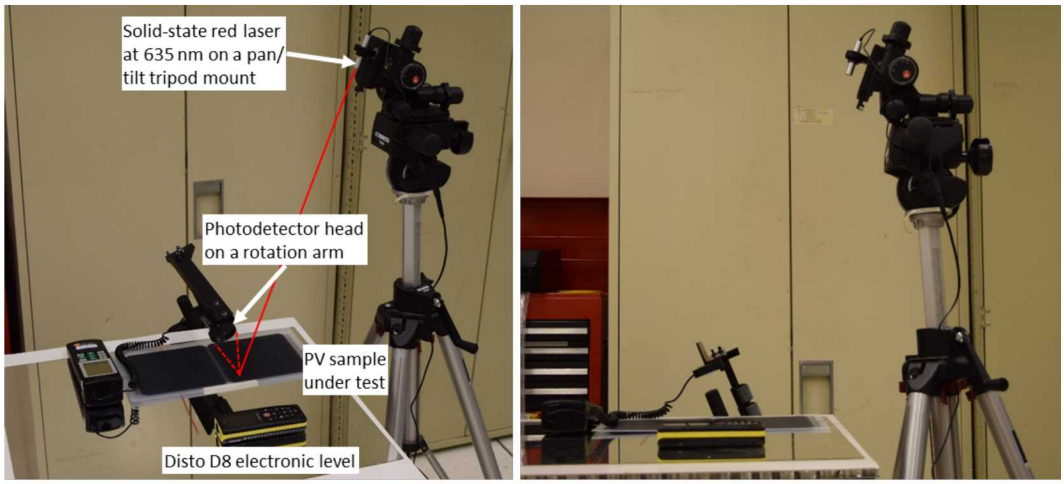

Figure 3-1. Measurement set-up for measuring reflectance from flat surfaces at varying angles of incidence.

During measurements, the PV samples were placed such that the reflectance was measured over the solar cell region; the bus lines (wires) were avoided. The modules were measured at five different points over the surfaces. All three modules were measured the same. The data were analyzed separately for each module and then combined to get an overall reflectance performance from the batch. One PV modules was taken outdoors to take photos of the sun reflection.

3.2. Results

Measured Surface Reflectance

Surface reflectance results are shown in Figure 3-2. Combined measurements are represented by blue dots, while the error bars represent 1-standard deviation from the three modules. The three modules showed very low reflectance, < 2% up to 80° angle of incidence. The performance was comparable to the deeply textured samples (from different manufacturers) previously measured by Sandia. Fresnel reflection equations scaled by an extinction parameter (due to large scattering) were fitted to the measured data. The curve fit is shown in red in Figure 3-2 with an R^2 value of 0.9984. The reflectance measured with the Surface Optics 410-Solar reflectometer showed an average total hemispherical reflectance of 11.5% (± 0.1%). The specular reflectance with the 410-Solar (at 20°

angle of incidence) showed < 0.5%. The reflectance data will be incorporated into the GlareGauge tool (formerly SGHAT developed by Sandia). GlareGauge is licensed to ForgeSolar (https://www.forgesolar.com).

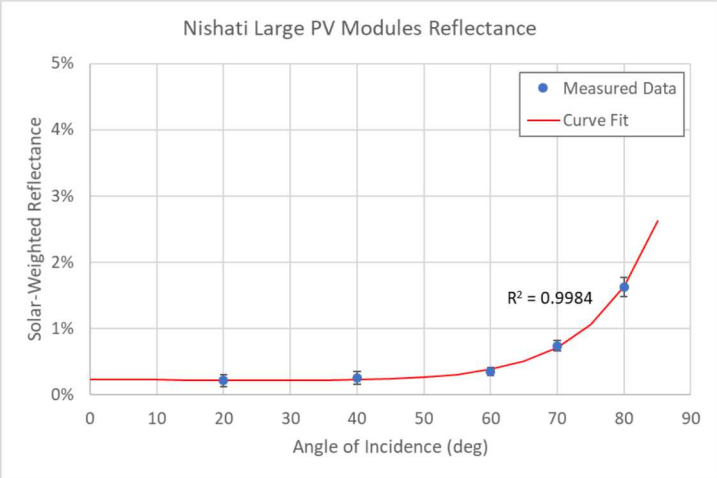

Figure 3-2. Measured solar-weighted reflectance vs. angle of incidence

On-Sun Reflection

One PV module (3405) was taken outdoors to collect images of the sun reflection. For comparison, a small PV module (different manufacturer) was also used to reflect the sun. Camera settings were kept constant for both images. As shown in Figure 3-3a, it was difficult to see the sun in reflection from the Nishati module. Reflections off the bus lines gave some indication of the sun reflection, but over the solar cells the sun reflection was not easy to see. The small module, Figure 3-3b, has a lightly textured polymer cover. In this case, the sun reflection (although scattered) can be seen easily.

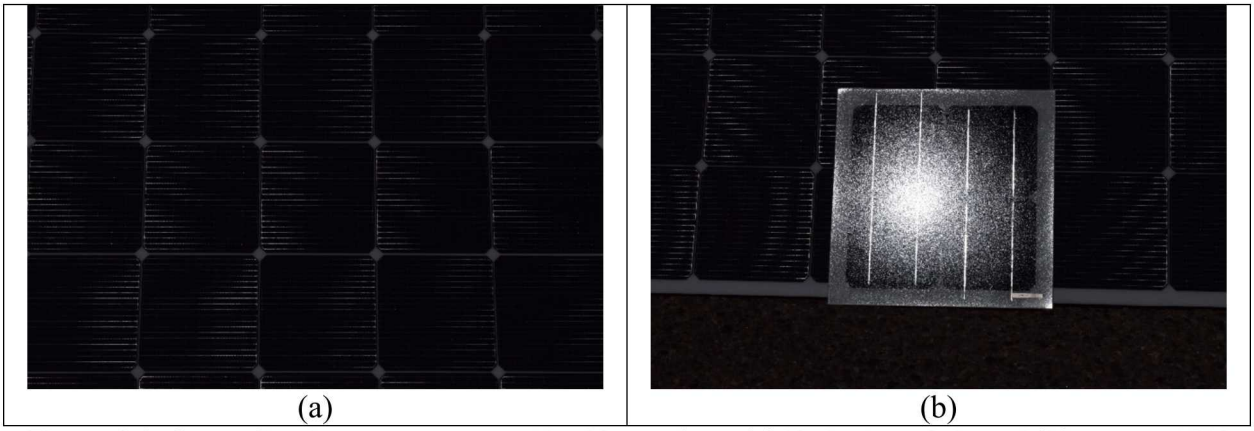

Figure 3-3. Sun reflection at near normal incidence from (a) Nishati module and (b) textured PV sample.

Interestingly, the Nishati samples do not have deeply textured covers as seen in other PV modules with low reflectance. The low reflectance and lack of deep texture could have advantages. The low reflectance can minimize glint and glare which cause potential hazards, especially to aircraft pilots flying over large solar installations. The lack of a deep texture could have benefits in terms of reduced soiling as compared to deeply textured surfaces. However, soiling studies on textured surfaces have not been yet done to make comparisons.

4. INDOOR CHARACTERIZATION

4.1. Flash Testing

Each module was flash tested on a Class AAA [2] Spire 4600 SLP one-sun simulator at Standard Test Conditions (STC) of 1000 W/m^2, 25°C and incident spectrum matched to Air Mass 1.5. IV curves were recorded in the forward direction, short-circuit current to open circuit voltage. All flash testing was performed prior to any solar exposure.

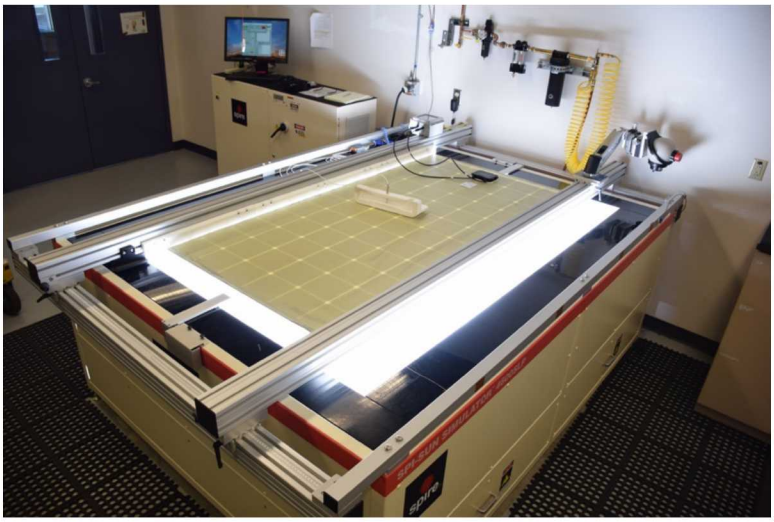

Figure 4-1. Nishati Prototype Endurance Module on Spire 4600 SLP

The shape of each IV curve was satisfactory. PVID's 3405 and 3406 displayed very modest cell-string mismatches, with small observable steps. In comparison, all strings in PVID 3507 appeared to be very well matched. See inset below in Figure 4-2. These results are consistent with electroluminescence imaging (Section 4.2).

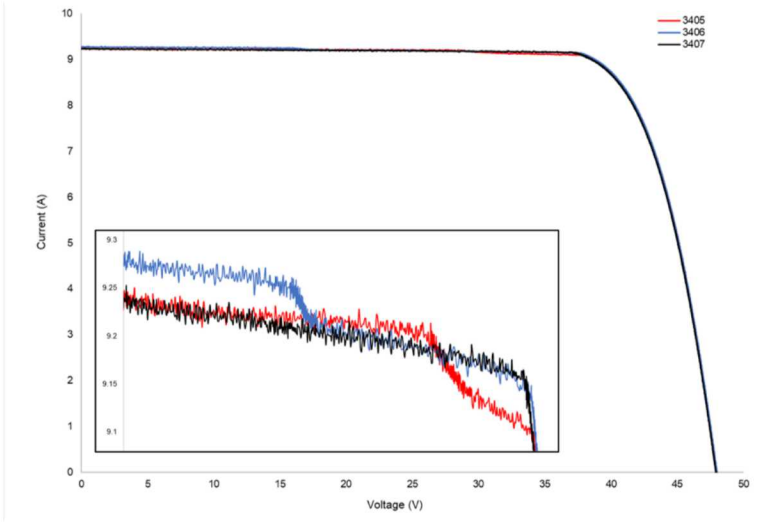

Figure 4-2. IV Curves from Flash Tester

Electrical performance at STC is shown below in Table 4-1. All measured parameters were within about 0.5% of the mean value, or lower. These results indicate that the observed string mismatch within 3405 and 3406 has negligible impact on the overall performance of the modules. Publicly

available specification sheet values for two commercial 72-cell modules in a similar power class are shown for comparison. The Nishati prototype Endurance modules perform in line with expectations for modules of this size and power class.

Table 4-1. STC Electrical Performance Compared to Commercial Modules

PVID #	Isc	Voc	Imp	Vmp	Pmp	FF (%)	Eff(%)	Ω @ Voc	Ω @ Isc
3405	9.24	47.92	8.85	39.47	349	79	17.8	0.469	436
3406	9.28	47.98	8.87	39.43	350	79	17.8	0.483	414
3407	9.24	47.91	8.85	39.32	348	79	17.8	0.478	361
JASolar[i]	9.54	47.05	8.99	38.39	345	77	17.8	-	-
Q-Cells[ii]	9.64	47.46	9.09	37.93	345	75	17.3	-	-

4.2. Electroluminescence

Electroluminescence imaging was performed in a custom dark chamber housing a Reltron EL camera. Images were recorded at voltage bias levels set such that current levels of 80% and 20% of Isc were reached. Required exposure times were short (9.6 and 38 seconds, respectively), consistent with the relatively high efficiency seen from flash testing.

Cell cracking visible, subjectively greater cell-to-cell variation visible in 3405 and 3406, consistent with small steps seen in flash test IV curves.

[i] JAM6(K)-72-345/PR
[ii] Q.PLUS L-G4.2 345

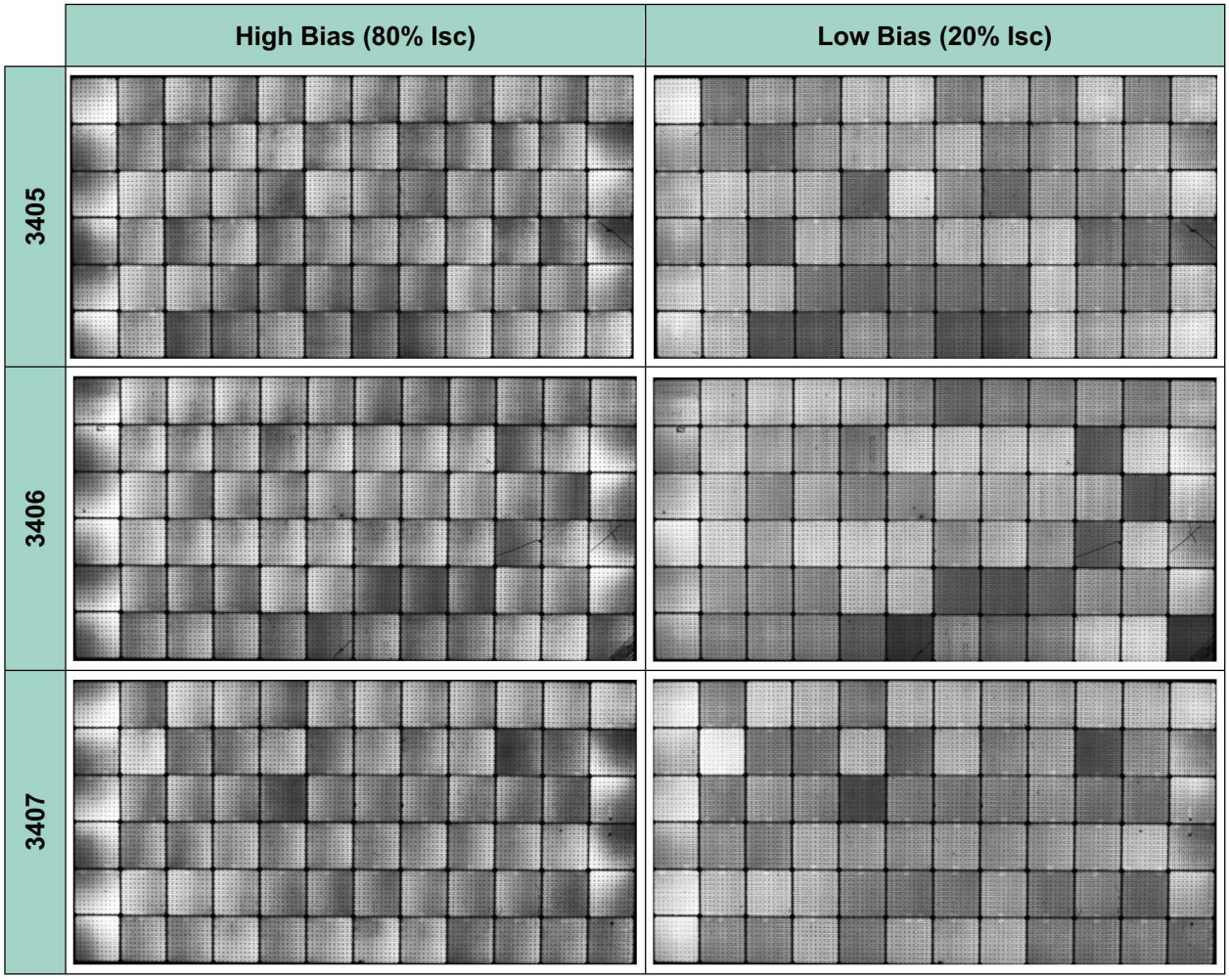

Figure 4-3. EL images for each module at High and Low bias

5. OUTDOOR CHARACTERIZATION TEST DETAILS

5.1. Instrumentation

Three Pt100 Resistance Temperature Detectors (RTD) were attached to the rear side of each module as shown in Figure 5-1. Positions used were similar to, but not exactly the same as specified by IEC 61853 [3]. Due to the honeycomb structural element, it was necessary to core each module to locate the RTDs as close as possible to the back of a cell (Figure 5-2).

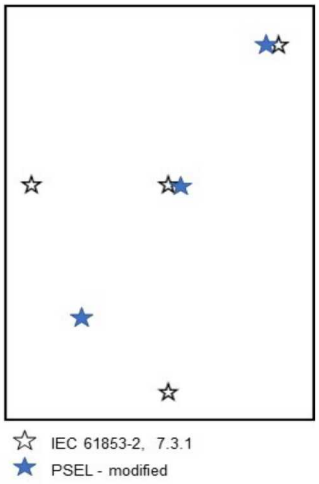

Figure 5-1. RTD locations on each module

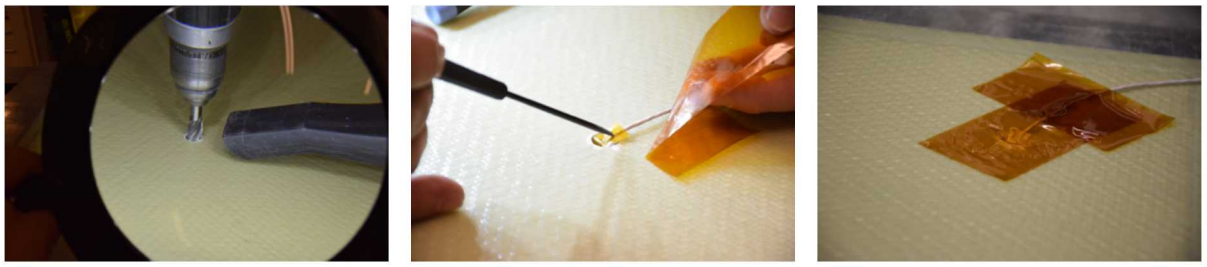

Figure 5-2. Coring and RTD placement

5.2. Tracker Mounting and Preconditioning

All three modules were mounted coplanar on a two-axis solar tracker in landscape orientation, shown below in Figure 5-3. Each module was connected to a custom current-voltage (IV) sweep system using the supplied leads. Once the modules were mounted to the test plane, the tracker was put into automatic Sun tracking mode, positioning each module normal to the Sun. Each module was held at maximum power by the IV system. IV sweeps (I_{sc} to V_{oc}) were performed every 2 minutes during daylight periods. During night time, the tracker was stowed at an azimuth of 180° and elevation of 45°. The modules were held normal to the Sun for approximately six weeks. Collected IV data was used to derive in-situ temperature coefficients, STC power ratings and model coefficients for the Sandia Array Performance Model [1]. Angle of Incidence (AOI) characterization was performed near the conclusion of the test period.

Figure 5-3. Test Devices mounted on two-axis solar tracker

5.3. Characterization and Analysis Methods

Characterization procedures followed those described in [4]. Analysis was performed using the "Simultaneous" solution method to the SAPM, described in [5]. These procedures are similar to those described in [4], with the exception that the constitutive equations for the SAPM are solved simultaneously for each model coefficient. This method has the advantage of determining temperature coefficients *in situ* using static data rather than dynamic. This has been shown to produce more relevant temperature coefficients for modules with slow thermal response.

AOI test and analysis procedures followed the Preferred Method described in [4]. The tracker was indexed in elevation only during the test and continued to track the Sun in azimuth. Indexing was from 0° to 85° in decreasing angular steps. The tracker was held at each angular offset while a minimum of five IV sweeps were measured. I_{sc} values used in the analysis were temperature corrected using the *in-situ* derived temperature coefficients and averaged for each angular offset. Diffuse irradiance was measured in the plane of array using a pyranometer equipped with a vertical shadow band. It should be noted that use of this measurement differs from similar procedures described in IEC 61853-2 [3], where diffuse irradiance is calculated from direct normal (DNI) and GNI.

5.4. Environmental Conditions During AOI Characterization

AOI characterization was performed simultaneously on all three modules. Characterization was performed near solar noon under clear sky conditions on two different days (8/13 and 8/20). Environmental conditions during each test are listed in Table 5-1. Peak-to-peak variation in GNI during the reported test periods was 12 W/m^2 or less (~1.2%). The ratio of DNI/GNI during the test met the minimum requirement (0.85). Values above 0.9 are preferred, but more uncommon during late summer owing to higher humidity.

Table 5-1. Environmental conditions during AOI characterization

Condition	8/13/18	8/20/18
Ambient Temp, °C	26.9	27.2
Wind Speed, m/s	2.5	2.1
Relative Humidity, %	28.8	34.2
DNI, W/m2	870	875
GNI, W/m2	1029	1034
DNI/GNI	0.85	0.85
Air Mass	0.88	0.92

6. OUTDOOR TEST RESULTS

6.1. Summary STC Performance

Summary electrical performance of each module under Standard Test Conditions (STC) are presented below in Tables 6-1 and 6-2. As mentioned in Section 5.3, STC parameters are determined from simultaneous, multivariate regression analysis of all outdoor data. This differs from indoor flash testing as described Section 4.1, in which test conditions are deterministically controlled. In contrast to indoor testing, there was significant variation between modules. Due to instrumentation issues, curves collected during non-ideal conditions were used in the analysis of PVID 3406. Consequently, this module underperformed the other modules. The effect is most pronounced in the in-situ derived temperature coefficients, in which coefficients for current (α-Isc and α-Imp) are unrealistically high. Consequently, the temperature coefficient for power (γ-Pmp) is unrealistically low. PVID 3405 performed the most closely to indoor testing and produced temperature coefficients in line with expectations. In the remainder of this section, response curves for PVID 3405 will be presented as representative.

Table 6-1. STC Electrical Performance Determined from Outdoor Tracker Testing

PVID #	Isc	Voc	Imp	Vmp	Pmp	FF (%)	n
3405	9.36	47.56	8.86	38.67	342.54	77	1.12
3406	9.13	47.23	8.63	38.33	330.71	77	1.05
3407	9.61	47.48	9.13	38.30	349.51	77	1.11

Table 6-2. *In-Situ* Derived Temperature Coefficients

PVID #	α-Isc (%/C)	β-Voc (%/C)	α-Imp (%/C)	β-Vmp (%/C)	γ-Pmp (%/C)
3405	0.052	-0.290	-0.026	-0.385	-0.42
3406	0.189	-0.271	0.109	-0.365	-0.26
3407	-0.031	-0.289	-0.114	-0.371	-0.49
JASolar[iii]	0.06	-0.30	-	-	-0.39
Q-Cells[iv]	0.04	-0.29	-	-	-0.40

6.2. Response to Irradiance and Air Mass

Isc response to Irradiance and Air Mass are shown below in Figure 6-1. In the plot on the left, measured Isc values are translated to a common reference condition of 25°C and Air Mass 1.5 and plotted against measured broadband irradiance in the plane of array (GPOA). This response is linear, in accordance with expectations. In the plot on the right, measured Isc is translated to a common reference condition of 25°C and 1000 W/m^2, normalized by Isc at STC conditions and plotted against air mass. This plot highlights a challenge with the data set used for this analysis. Most of the data is concentrated at low air mass, between 0.8 and 2, while data is scare at higher values up to AM 5. This is due to the lack of clear sky conditions occurring during morning and evening hours during the test period. Consequently, air mass response rises to a peak higher than

[iii] JAM6(K)-72-345/PR
[iv] Q.PLUS L-G4.2 345

typically expected for silicon devices. A longer test with more ideal conditions would produce an Air Mass response plot with better uncertainty in the high AM range. However, even with the lack of high AM data, response between the low end of the test and ~AM 3 is in line with expectations.

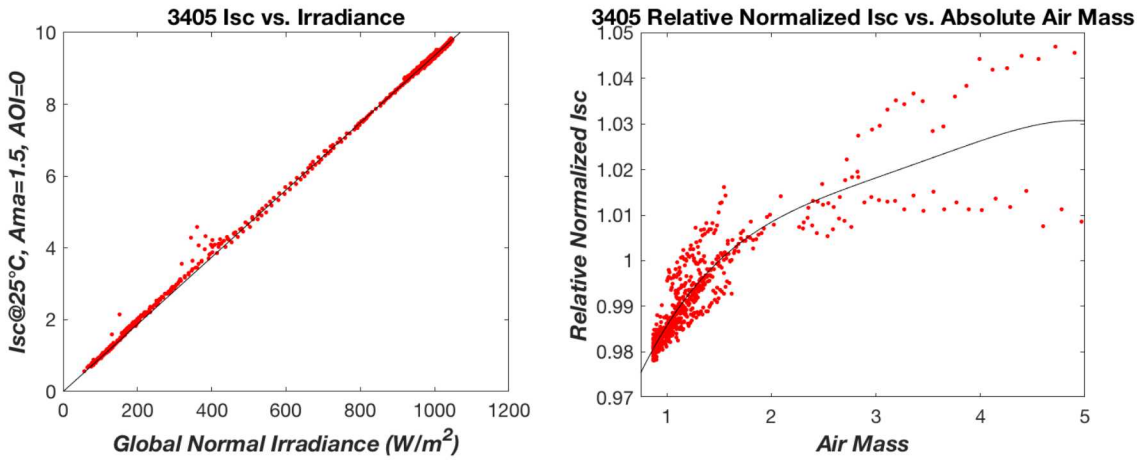

Figure 6-1. Isc response of PVID 3405 as a function of Irradiance and Air Mass

6.3. Effective Irradiance (Ee)

Isc, calibrated against irradiance and air mass, is used to determine the Effective Irradiance (Ee) which is then used in all subsequent analysis. Response is shown below in Figure 6-2 for currents and voltages. Isc is by definition linear against Ee. Imp follows a slight polynomial behavior as expected. Voltages display a characteristic logarithmic behavior that rises quickly up to Ee=0.2-0.3 and the flattens out, again in line with expectations.

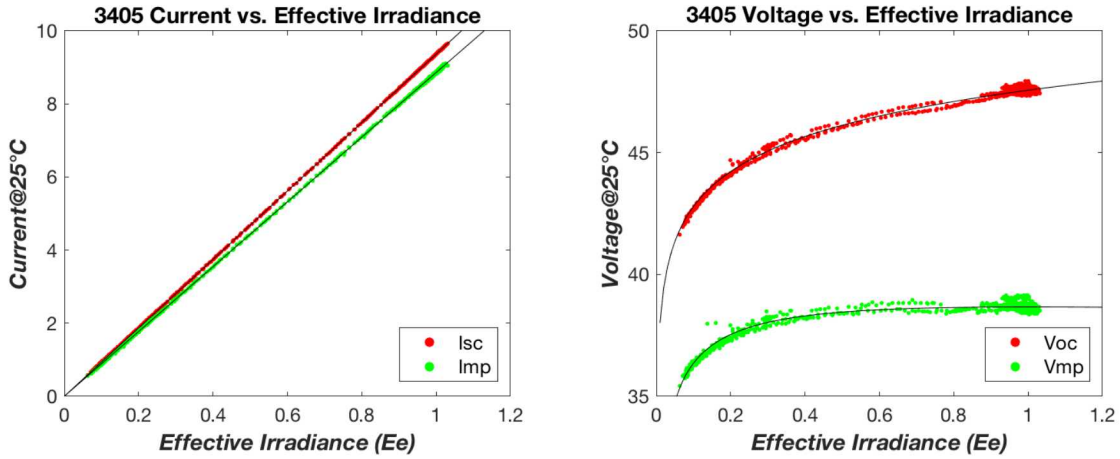

Figure 6-2. Current and Voltage response of PVID as a function of Effective Irradiance

6.4. Temperature Coefficients

In-situ derived temperature coefficients are show below in Figure 6-3. Response is in line with expectations. Isc was seen to rise very slightly with increasing temperature, whereas Imp decreased very slightly. Voltages consistently decrease with increasing temperature. Significant scatter in the data is apparent in the plot of Isc at low temperatures. This is due to these data points generally occurring under cloudy, low irradiance conditions. Cloudy data is not used in the derivation of α-Isc

but is shown here for comparison to the subsequent plots, as cloudy data is used to derive the remaining temperature coefficients.

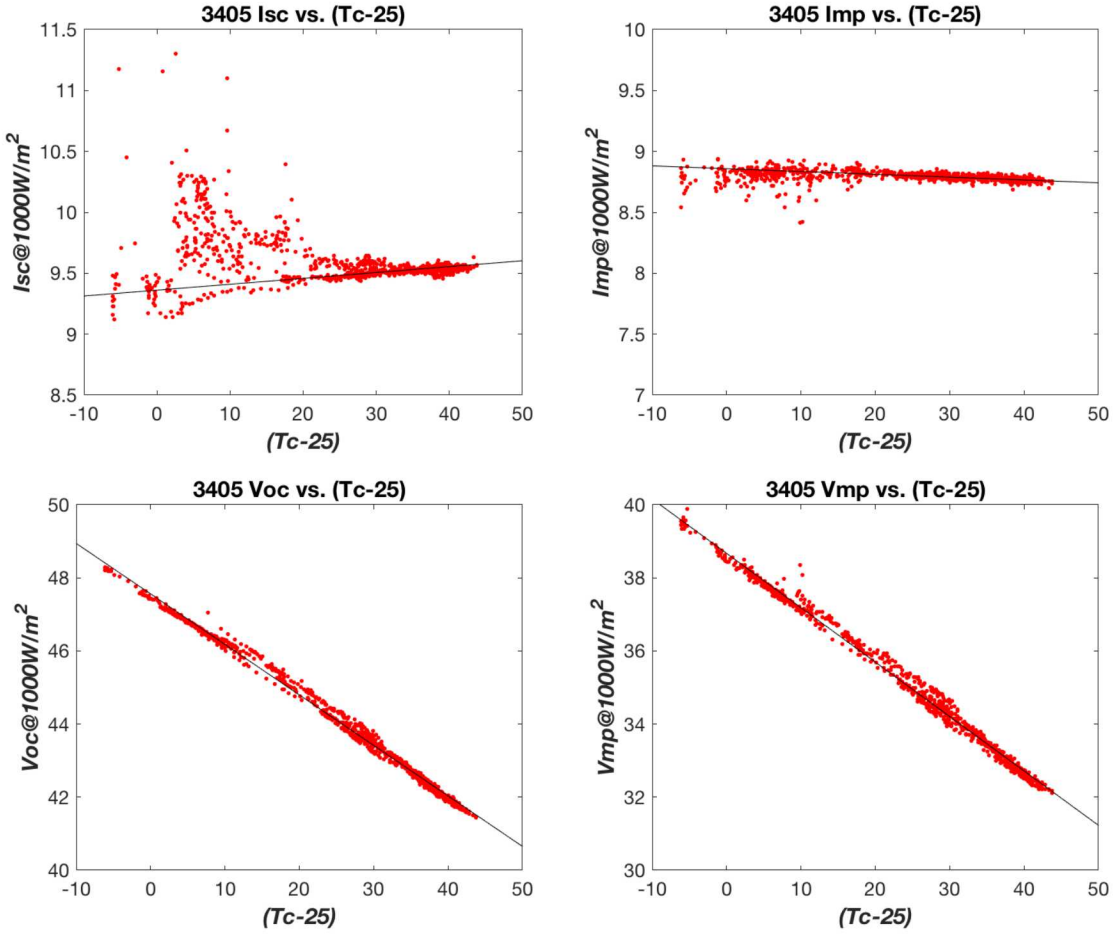

Figure 6-3. *In-situ* derived temperature coefficients for PIVD 3405.

6.5. Thermal Model and Normal Module Operating Temperature

A thermal model for each module was calibrated using measured module and ambient temperature, wind speed and broadband POA irradiance. An example of the model is shown below in Figure 6-4 for PVID 3405. The majority of the data is clustered between 1 and 4 m/s.

Table 6-3. Normal Module Operating Temperature (NMOT)

PVID #	a	b	NMOT (°C)
3405	-3.392	-0.1057	44.2
3406	-3.405	-0.1255	43.4
3407	-3.352	-0.1198	44.8
JASolar[v]	-	-	42.6
Q-Cells[vi]	-	-	42.6

[v] JAM6(K)-72-345/PR
[vi] Q.PLUS L-G4.2 345

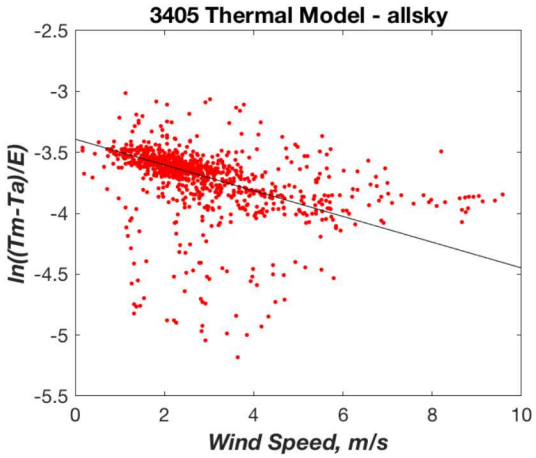

Figure 6-4. Thermal Model for PVID 3405

The calibrated thermal model was then used to calculate normal module operating temperatures (NMOT) for each module, shown in Table 6-3 along with coefficients for the thermal model. NMOT is shown for two comparable utility scale modules for comparison. It should be noted that the value presented here is calculated from published specification sheet values for the conceptually similar Normal Operating Cell Temperature (NOCT).

6.6. Model parameters applied to power

For validation, model results were used to calculate power as a function of effective irradiance and cell temperature. As can be seen, there is excellent agreement between calculated results and measured results. This indicates that a simple linear power model may be used to estimate system power for design purposes.

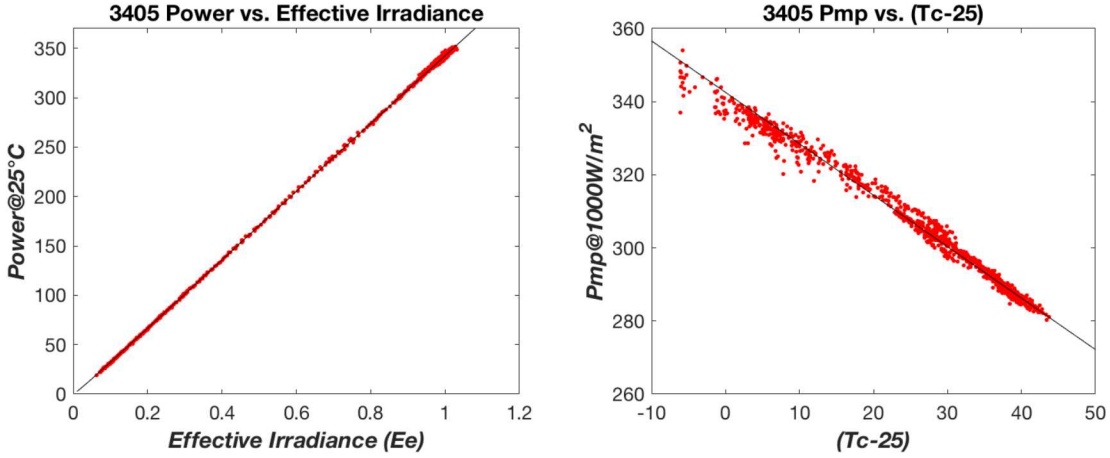

Figure 6-5. Inter-day variability observed for two commercial modules

6.7. Angle of Incidence Characterization

Angle of incidence (AOI) response proved to be the one area in which performance of the prototype modules deviated substantially from that of typical utility PV modules. The results of this characterization are shown below in Figure 6-6. AOI response for a typical utility PV module is shown for reference. Response of the commercial module is typical of modules using a traditional glass coversheet. Even highly differentiated modules will have slight deviation from this curve when

displayed full scale. Typical modules will display flat response up to about 50°, after which response will drop. A "knee" in the response curve is often observed in the range of 65-70°. As the degree of reflection increases at steep incidence angles, response typically plunges toward 0. In contrast, the polymeric front surface of the prototype modules appears to dramatically reduce reflection losses, and hence displays significantly improved behavior relative to glass modules. Considering the reflective properties highlighted in Section 2, this behavior should not come as a surprise. However, this type of response is relatively unknown in the PV industry and may prove to be a strong differentiating feature for certain types of deployment scenarios. Given the novelty and potential significance of this behavior, it is recommended that these measurements be repeated for validation.

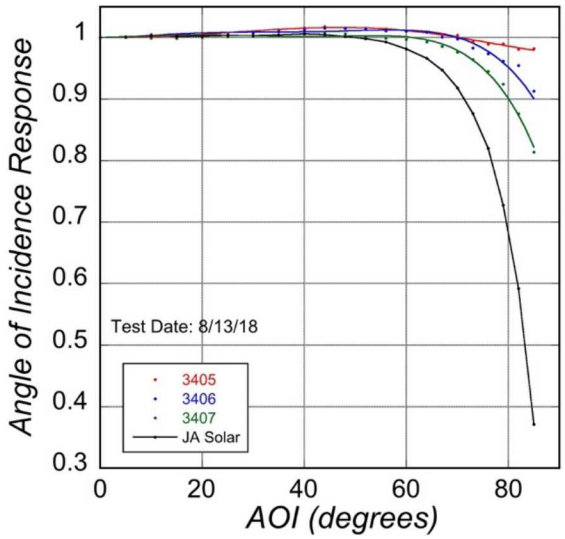

Figure 6-6. Angle of Incidence Response

REFERENCES

[1] King, D.L., E.E. Boyson, and J.A. Kratochvil, Photovoltaic Array Performance Model, SAND2004-3535, Sandia National Laboratories, Albuquerque, NM, 2004.

[2] IEC 60904-9:2017, "Photovoltaic devices – Part 9: Solar simulator performance requirements"

[3] IEC 61853-2:2016, "Photovoltaic (PV) module performance testing and energy rating – Part 2: Spectral responsivity, incident angle and module operating temperature measurements"

[4] Bruce H. King, Clifford W. Hansen, Dan Riley, Charles D. Robinson, Larry Pratt, "Procedure to Determine Coefficients for the Sandia Array Performance Model (SAPM)," SAND2016-5284, Sandia National Laboratories, Albuquerque, NM, 2016.

[5] B. H. King, "CIGS Performance Analysis: Alternative Method to Fit the Sandia Array Performance Model," presented at *The 5th PV Performance Modeling Workshop*, SAND2016-4658C. (https://pvpmc.sandia.gov/download/5240/)

APPENDIX A. REFLECTION TEST RESULTS

A.1. Measured Reflection

AOI	Average R, %	St Dev R	2 – St Dev R
20	0.216291%	0.09%	0.18%
40	0.253184%	0.10%	0.19%
60	0.352125%	0.06%	0.12%
70	0.744199%	0.08%	0.15%
80	1.628627%	0.15%	0.30%

A.2. Curve Fit to Fresnel Equation

AOI	R, %
0	0.22951
5	0.229168
10	0.228188
15	0.226717
20	0.225033
25	0.223598
30	0.223156
35	0.224885
40	0.230634
45	0.243324
50	0.267576
55	0.310758
60	0.38473
65	0.508833
70	0.715176
75	1.058395
80	1.634698
85	2.621707

APPENDIX B. PROCESSED OUTDOOR TEST RESULTS

B.1. SAPM Coefficients[vii], 3405

Coefficient	Value	Details
Ns	72	Cells in series
Np	1	Cell strings
Isco	9.361188339	Isc at STC, (A)
Voco	47.56025529	Voc at STC, (V)
Impo	8.858138753	Imp at STC, (A)
Vmpo	38.66945795	Vmp at STC, (V)
α-Isc	0.000515374	Isc temperature coefficient, (1/°C)
α-Imp	-0.000261124	Imp temperature coefficient, (1/°C)
C_0	1.001721984	Coefficients relating Imp to Effective Irradiance, (dimensionless)
C_1	-0.001721984	
β-Voc	-0.138159788	V_{oc} temperature coefficient, (V/°C)
β-Vmp	-0.148804489	V_{mp} temperature coefficient, (V/°C)
n	1.120575159	Cell diode factor (dimensionless)
C_2	0.004048711	Coefficients relating Vmp to Effective Irradiance, (C_2, dimensionless; C_3, 1/V)
C_3	-7.247080017	
a_0	0.925265645	Polynomial coefficients for spectral (Airmass), $f_1(AM_a)$
a_1	0.091138915	
a_2	-0.037559962	
a_3	0.007520637	
a_4	-0.000562223	
ΔT	3	Temperature difference between cell & module @ 1000 W/m^2
fd	1	Fraction of diffuse POA used by the module
a	-3.39174055	Coefficients relating Wind Speed (WS), Irradiance (GPOA) and Ambient Temperature (T_a) to Module Temperature (T_m)
b	-0.105669394	

[vii] This table is abbreviated. Coefficients that are now considered obsolete have been omitted. Polynomial coefficients for the AOI $f_2(\theta)$ function are presented in A2.

B.2. Polynomial AOI Function, $f_2(\theta)$

Coefficient	3405	3406	3407
b_0	1	1	1
b_1	0	0	0
b_2	9.16088E-06	6.07154E-05	5.36921E-05
b_3	4.38139E-07	-3.13651E-06	-3.36691E-06
b_4	-1.41543E-08	5.96974E-08	7.13376E-08
b_5	8.63284E-11	-3.89506E-10	-5.00851E-10

B.3. AOI Lookup Table

AOI	Normalized I_{sc}		
	3405	3406	3407
0	1.0000	1.0000	1.0000
5	1.0011	1.0013	1.0002
10	1.0048	1.0032	0.9993
15	1.0051	1.0031	0.9987
20	1.0057	1.0021	1.0001
25	1.0073	1.0046	1.0012
30	1.0082	1.0074	1.0021
35	1.0126	1.0095	1.0043
40	1.0157	1.0129	1.0068
44	1.0177	1.0152	1.0088
48	1.0156	1.0148	1.0060
52	1.0152	1.0139	1.0019
56	1.0143	1.0110	0.9994
60	1.0108	1.0105	0.9972
64	1.0085	1.0092	0.9929
67	1.0054	1.0009	0.9855
70	1.0037	0.9976	0.9761
73	0.9927	0.9830	0.9643
76	0.9894	0.9735	0.9449
79	0.9897	0.9615	0.9244
82	0.9809	0.9545	0.8758
85	0.9822	0.9131	0.8135

DISTRIBUTION

Email—External[redacted]

Name	Company Email Address	Company Name
Mike Tupper	mtupper@nishati-us.com	Nishati
Richard Schilke	rschilke@nishati-us.com	Nishati
Andrew Dawson	Andrew.Dawson@ee.doe.gov	US-DOE

Email—Internal

Name	Org.	Sandia Email Address
Technical Library	9536	libref@sandia.gov

This page left blank

This page left blank

Sandia National Laboratories

Sandia National Laboratories is a multimission laboratory managed and operated by National Technology & Engineering Solutions of Sandia LLC, a wholly owned subsidiary of Honeywell International Inc. for the U.S. Department of Energy's National Nuclear Security Administration under contract DE-NA0003525.